Research Article | Vol. 28, No. 4 / 17 February 2020 / Optics Express 5134
Optics EXPRESS

Compact silicon photonic hybrid ring external cavity (SHREC)/InGaSb-AlGaAsSb wavelength-tunable laser diode operating from 1881-1947 nm

JIA XU BRIAN SIA,[1] WANJUN WANG,[1] ZHONGLIANG QIAO,[1] XIANG LI,[1] XIN GUO,[1] JIN ZHOU,[1] CALLUM G. LITTLEJOHNS,[1,2] ZECEN ZHANG,[1] CHONGYANG LIU,[3] GRAHAM T. REED,[1,2] AND HONG WANG[1,*]

[1]*School of Electrical and Electronic Engineering, Nanyang Technological University, 50 Nanyang Avenue, 639798, Singapore*
[2]*Optoelectronics Research Centre, University of Southampton, Southampton SO17 1BJ, UK*
[3]*Temasek Laboratories, Nanyang Technological University, 50 Nanyang Drive, 637553, Singapore*
[*]*ewanghong@ntu.edu.sg*

Abstract: In recent years, the 2 μm waveband has been gaining significant attention due to its potential in the realization of several key technologies, specifically, future long-haul optical communications near the 1.9 μm wavelength region. In this work, we present a hybrid silicon photonic wavelength-tunable diode laser with an operating range of 1881-1947 nm (66 nm) for the first time, providing good compatibility with the hollow-core photonic bandgap fiber and thulium-doped fiber amplifier. Room-temperature continuous-wave operation was achieved with a favorable on-chip output power of 28 mW. Stable single-mode lasing was observed with side-mode suppression ratio up to 35 dB. Besides the abovementioned potential applications, the demonstrated wavelength region will find critical purpose in H_2O spectroscopic sensing, optical logic, signal processing as well as enabling the strong optical Kerr effect on Si.

1. Introduction

Over the past decades, exuberant innovation in the telecommunications industry have led to the development of low-loss single-mode fiber (SMF) [1], erbium-doped fiber amplifiers (EDFAs) [2], wavelength division multiplexing (WDM) techniques [3], and more recently, digital coherent transmission [4]; pushing the record transmission capacity within a factor of 2 of the nonlinear Shannon limit [5]. While mode-division multiplexing in few-modes fiber (FMF) can increase the spectral efficiency of the 1.55 μm band [6], high modal dispersion in FMF renders the approach challenging for practical applications [7,8]. There is a pressing need for the development of a high-capacity physical layer technology to address the ever-growing demand for information in the long run. Breakthroughs in the hollow-core photonic-bandgap fiber (HC-PBGF) [9–12] and thulium-doped fiber amplifier (TDFA) [13,14] have highlighted the prominence of the 2 μm waveband for future long-haul optical communications. By propagating 99.8% of light in air, HC-PBGFs can achieve low latency and large capacity transmission (low nonlinearity) [9]. Because of reduced infrared 'multiphonon' absorption via lower modal overlap with glass [10], it has been predicted that near 1.9 μm, HC-PBGFs will display loss levels comparable to that of the SMFs at the 1.55 μm waveband [11,12]. Conveniently, the low-loss window of the HC-PBGFs (~ 1.9 μm) coincides closely with the operation bandwidth of the TDFA [13,14]. Instances of viability in terms of future optical communications include the error-free 100 Gbit/s WDM transmission over HC-PBGF [15] as well as dense WDM transmission by means of arrayed

#383524 https://doi.org/10.1364/OE.383524
Journal © 2020 Received 25 Nov 2019; revised 25 Jan 2020; accepted 26 Jan 2020; published 10 Feb 2020

Optics EXPRESS

waveguide grating [16]. Moreover, the applications of the 2 μm waveband are not restricted to fiber communications. Developments into the waveband can lead to the culmination of several other key technologies; gas sensing [17], free-space communications [18], LIDAR [19], etc.

Silicon photonics (SiPh) is a decisive technology, by exploiting advanced CMOS process for large-yield mass fabrication, high-density photonic integration can be realized. To date, most fundamental components [20–28] have been demonstrated on the platform to great effect. Recent trend suggests an extension of SiPh from the O/C-band to the 2 μm waveband to enable a wide range of applications [29]. Instances include the development of high-speed silicon photonic modulators [30], photodetectors [31] and passive components [32–35]. The realization of the laser source, however, has been more challenging; Si is a poor emitter of light. Hybrid/heterogenous [36] silicon photonic diode lasers enable additional degrees of freedom as compared to III - V lasers by combining the best of both worlds. SiPh offers low propagation loss and high integration densities while III - V material contributes high gain values [37] and the flexibility for bandgap engineering via changes in material composition [38], realizing high performance, novel light sources; examples are the high power, sub-kHz linewidth heterogenous silicon laser [39] as well as hybrid/heterogenous silicon lasers that operate in the spectroscopically imperative wavelength region above 2 μm [40]. Hybrid integration allows for III - V and silicon to be individually optimized, while the heterogenous approach enables compact footprint in addition to demonstrating potential for high-volume production [36].

Wavelength-tunable lasers serve as an integral component in current WDM systems. By replacing an array of single-wavelength DFB lasers with a tunable laser, reduction in system complexity, wavelength contention and inventory cost can be achieved. While not exhaustive, other applications of the tunable laser include identification of gas species via specific wavelength absorption features [17] as well as enabling the differential absorption LIDAR technique [19]. The high-index contrast of the SOI platform facilitate micro-rings resonators with tight bending radius, as such, dual-ring SHREC architectures can achieve large free spectral range (FSR) (~140 nm), paving the way for broadly tunable lasers.

Thus far, impressive work on SHREC wavelength-tunable laser diodes have been achieved near the C-band [41–46]; examples include wide tuning range [42], increased power and operating temperature [44], large side-mode suppression ratio (SMSR) [45] and shifting of tuning range from C- to L-band [46]. However, there seems to be lesser development around the 2 μm waveband [47,48]. In this work, we designed our semiconductor optical amplifier (SOA) to be based on $In_{0.2}Ga_{0.8}Sb$ single quantum well (SQW), sandwiched by $Al_{0.25}GaAsSb$ barriers resulting in 1.26% of compressive strain. The emission of the SOA provides good compatibility ($1800 \leq \leq 2000$ nm) with the HC-PBGF [11,12] and TDFA [13,14]. The main objective of this work is to address the need for development from 1800-2000 nm through the integration of appropriately designed SHREC and SOA chips. Other than the possibility of supporting the applications as mentioned earlier, this wavelength region critically coincides with the "prime spot" for implementation of optical logic and signal processing [29], strong optical Kerr effect on Si [49] as well as the "absorption window" of H_2O vapor [50]. Favorable on-chip output power of up to 28 mW with a tunable range of 1881-1947 nm is demonstrated. This work is organized as follows. Firstly, we provide fundamental theoretical basis and critical experimental characterization of the SHREC. Next, the designed epitaxial structure of the SOA and measured spontaneous emission spectra are shown. Design and analysis of edge-coupling between the SHREC and III - V waveguide is presented. Finally, the performance of the laser is experimentally characterized and discussed.

2. SHREC wavelength tunable laser diode

Figure 1 illustrates the 3-D schematic of the SHREC/InGaSb-AlGaAsSb wavelength-tunable laser diode along with the labelled coordinates that will be standardized in this work.

Optics EXPRESS

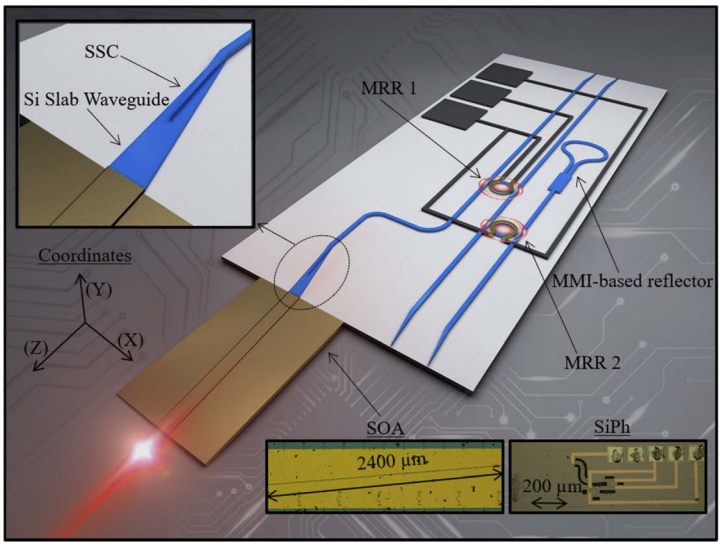

Fig. 1. 3-D schematic of the SHREC wavelength-tunable laser diode; inset shows the micrograph images of the SOA, SiPh SSC and wavelength-tunable Vernier cavity.

The laser cavity is realized by edge-coupling the SOA to the wavelength-tunable Vernier cavity via the Si slab waveguide and the spot-size converter (SSC) [43]; the SOA provides optical gain while the wavelength-tunable cavity enables wavelength-selective feedback by means of the Vernier effect. The lasing output occurs at the facet of the SOA as indicated. The wavelength-tunable Vernier cavity consists of 2 micro-ring resonators (MRRs) and a multimode interference (MMI)-based reflector. Thermo-optic phase shifters are mounted on top of the MRRs to enable thermal control of the lasing wavelength. The micrograph images of the SOA, Si, slab waveguide, SSC and wavelength tunable Vernier cavity are shown in the inset of Fig. 1.

The SiPh chip is fabricated on the 220 nm silicon-on-insulator (SOI) platform via a standard CMOS process. The strip waveguide (0.6×0.22 μm^2) propagation loss is experimentally characterized to be 3 dB/cm. A low-confinement silicon slab waveguide (6×0.07 μm^2) at the facet of the SSC is utilized to ensure close overlap with the optical field of the SOA. The radii of the MRRs are designed to be 16.8 (MRR1) and 18.2 μm (MRR2), corresponding to FSRs of approximately 8.9 nm (740 GHz) and 8.5 nm (706 GHz) respectively. By considering a MRR-bus waveguide coupling gap of 180 nm, the Q-factor of the MRRs is experimentally characterized to be 4800. After the waveguide fabrication steps, 1.2 μm of SiO_2 cladding is deposited followed by 120 nm of TiN for the heater and 2 μm of Al for routing. The heater efficiency is determined to be 6.2 mW/nm.

2.1. Vernier filter

One can define the power transmittance spectra of the MRRs as (1), where κ is the electric field coupling coefficient between the MRR and the bus waveguide, α is the loss coefficient of the waveguide, and θ is the phase change incurred in the lightwave after propagating one round in the MRR.

$$P_{ring\ 1,2} = \left|\frac{-\kappa^* \kappa \sqrt{\alpha}\exp(j\sqrt{\theta_{ring\ 1,2}})}{1-(\sqrt{1-|\kappa^2|})^*(\sqrt{1-|\kappa^2|})^*\alpha\exp(j\theta_{ring\ 1,2})}\right|^2 \quad (1)$$

Shown in the lower half of Fig. 2(a) is the theoretical transmittance spectra of the MRRs when zero heater power is applied on the phase shifters ($H_{MRR1} = H_{MRR2} = 0$ mW). The theoretical

Optics EXPRESS

transmittance spectra of the Vernier filter, shown in the upper half of Fig. 2(a), can be computed as a product of the power transmittance spectra of the 2 MRRs. Modal transmittance difference (MTD), the extent of transmittance difference between the main and adjacent peak of the Vernier transmittance spectra, is an important index of single-mode stability, the higher the value, the greater the selectivity of the wavelength tunable Vernier cavity [41], facilitating lasing by mode competition, a feature that will not be possible in a single MRR filter configuration. While the MTD and maximum tunable range of the wavelength-tunable Vernier filter can be increased by decreasing the radius of the MRR [41], one will be limited by the diffraction limit. The MRR-bus waveguide coupling gap is another design parameter that affects the MTD; by increasing the coupling gap, the MTD will increase, but however, the drop efficiency of the tunable laser will decrease leading to a rise in threshold current. Through the thermo-optic effect implemented via the TiN heaters (H_{MRR1}, H_{MRR2}), one will be able to control the wavelength of lowest loss through the overlap of 2 MRR resonant peaks, subsequently, the cavity longitudinal mode which most closely matches the Vernier transmittance peak will determine the lasing wavelength via mode competition. The optical single-trip length of the SiPh chip and SOA are calculated to be 5490 μm and 8640 μm respectively; the FSR of the cavity longitudinal mode is 0.13 nm (11 GHz). With regards to the design parameters indicated in Fig. 2(a), theoretical calculations imply that the Vernier filter will have an MTD of 8.34 dB and a maximum tunable range of 1843-1983

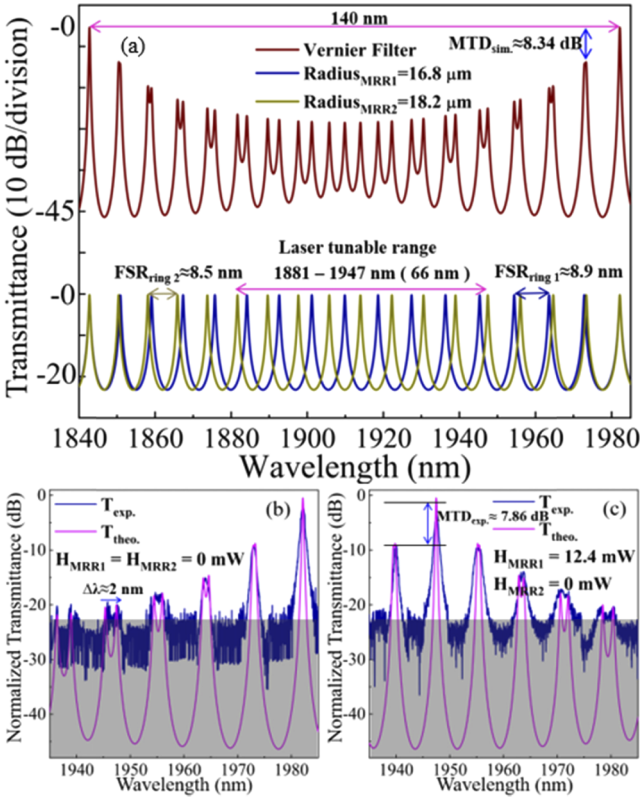

Fig. 2. (a) The red, blue and yellow lines indicate the power transmittance spectra of the Vernier filter, MRR 1, 2 respectively when $H_{MRR1} = H_{MRR2} = 0$ mW. (b) Measured and theoretical Vernier power transmittance spectra (1935-1985nm) when $H_{MRR1} = H_{MRR2} = 0$ mW. (c) Measured and theoretical Vernier power transmittance spectra (1935-1985nm) when $H_{MRR1} = 12.4$ mW, $H_{MRR2} = 0$ mW.

Optics EXPRESS

nm (140 nm). The experimentally obtained operation bandwidth of this work is indicated as well (Fig. 2(a)).

The measured and theoretical transmittance of the Vernier filter when $H_{MRR1} = H_{MRR2} = 0$ mW and $H_{MRR1} = 12.4$ mW, $H_{MRR2} = 0$ mW is shown in Figs. 2(b) and (c) respectively. The measurement was conducted from 1935-1985 nm due to the maximum tuning range of our light source. When $H_{MRR1} = 12.4$ mW, $H_{MRR2} = 0$ mW, we are able to red-shift the resonant wavelength of MRR 1 by 2 nm. Consequently, the resonant wavelengths of the 2 MRRs are overlapped at $\lambda \approx 1947$ nm with an MTD of 7.86 dB; $\lambda \approx 1947$ nm is the longest demonstrated lasing wavelength in this work. The loss at $\lambda \approx 1947$ nm (Loss (Vernier)$_{\lambda \approx 1947nm}$) is 1.379 dB (Fig. 2(c)). The experimental data is shown to resemble the theoretical expectation closely in Figs. 2(b) and (c); shaded areas indicate the noise floor of our detector.

2.2. MMI-based reflector

The 1 × 2 MMI structure was used in the reflector due to the its fabrication tolerance; by closing the loop at the double output end of the 1 × 2 MMI, a reflector can be formed (Fig. 1). The MMI width, length, gap between output tapers, taper length and taper width are designed to be 6, 24.2, 3.14, 20, 1.35 μm respectively as shown in Fig. 3(a). In order to characterize the single trip insertion loss of the MMI-based reflector, the MMI coupler is cascaded over 4 stages. The measured normalized transmittances at $\lambda \approx 1947$ nm shown in Fig. 3(b). The insertion loss (Loss (MMI)$_{\lambda \approx 1947nm}$) is experimentally characterized to be 0.538 dB. Due to the limited tuning range of our light source, we are unable to measure the operation bandwidth of the MMI over the demonstrated operation region of this work, nevertheless, we show the simulated operation bandwidth of the MMI in Fig. 3(c). The fabricated MMI has a simulated 0.25-dB ($BW_{0.25dB}$) and 0.5-dB ($BW_{0.25dB}$) bandwidth of 1859-1965 nm and 1840-1990 nm respectively; ($BW_{0.25dB}$) and ($BW_{0.25dB}$) refers to the spectral width corresponding to 0.25 and 0.5 dB below the peak transmittance value of the MMI.

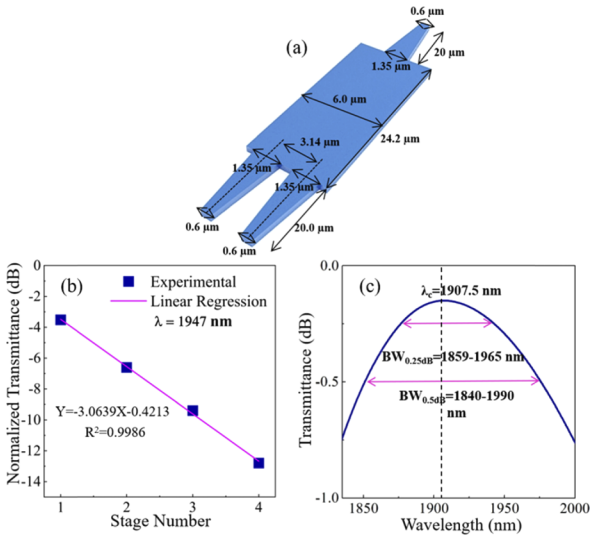

Fig. 3. (a) 3-D schematic of MMI coupler with associated physical parameters. (b) Measured linear fit for 1 × 2 MMI over 4 stages. (b) Simulated operation bandwidth of the 1 × 2 MMI.

Optics EXPRESS

As a reference, the estimated round-trip insertion loss of the wavelength-tunable Vernier cavity at $\lambda \approx 1947$ nm is experimentally characterized to be (Loss (Cavity)$_{\lambda\approx1947nm}$= [2 × Loss (Vernier)$_{\lambda\approx1947nm}$] + [2 × Loss (MMI)$_{\lambda\approx1947nm}$]) =3.834 dB.

2.3. InGaSb-AlGaAsSb SOA

The epitaxial structure (Fig. 4(a)) designed for the fabrication of the SOA was grown on a (100) n-GaSb substrate via molecular beam epitaxy (MBE) [51].

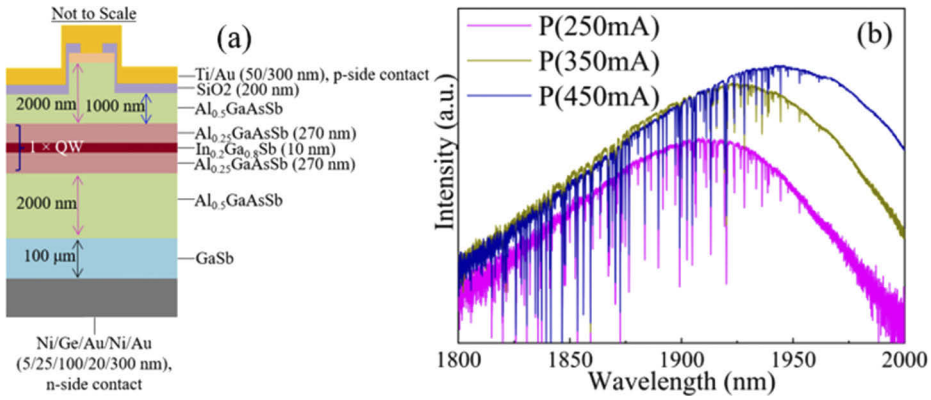

Fig. 4. (a) Epitaxial structure of InGaSb-AlGaAsSb SOA (x-y plane). (b) Measured spontaneous emission spectra of the InGaSb-AlGaAsSb SOA at I_{bias} = 250, 350, 450 mA.

It comprises of a 10 nm-thick $In_{0.2}Ga_{0.8}Sb$ single quantum well (1.26% compressive strain) with a 270 nm-thick $Al_{0.25}GaAsSb$ barrier on both sides. The cladding is composed of 2000 nm-thick $Al_{0.5}GaAsSb$ layers. The barrier, cladding layers are latticed-matched to the GaSb substrate. The SOA, as shown in Fig. 4, has a similar fabrication process to our prior work [52]. The ridge (6.4 × 1.0 μm^2) was defined using UV lithography and wet chemical etching. SiO_2 deposition was carried out via the plasma enhanced chemical vapor deposition (PECVD) process for injection current confinement. A contact window at the center of the ridge was defined by means of UV lithography and a buffered oxide etch (BOE) process. To enable responsive thermal control during laser operation, reduce series resistance, as well as facilitate cleaving, mechanical polishing was carried out on the GaSb substrate; The resultant thickness of the epitaxial structure is 100 μm. Ti/Au and Ni/Ge/Au/Ni/Au layers are evaporated to form the p and n-side ohmic contacts respectively. A heat sink was bonded to the n-side contact. The cross-section of the SOA is depicted at the inset of Fig. 4. The waveguide is angled at 4.5° to suppress Fabry-Perot (F-P) oscillations within the SOA; F-P oscillation at the SOA can reduce the stability of the tunable laser by decreasing the MTD of the Vernier filter [44]. Figure 4(b) shows the spontaneous emission spectra of the SOA at I_{bias} = 250, 350 and 450 mA; the output is obtained from the facet of the waveguide. The spectrum resembles the spontaneous emission measured in our previous work [53], implying that unwanted reflections in the SOA has been extensively subdued. The epitaxial structure grown in this work is designed to operate near the 1.9 μm wavelength region.

Due to the fact that the 1 × 2 MMI structure is wavelength-dependent, there is a need to ensure that the operation bandwidth of the MMI and SOA coincides; $BW_{0.25dB}$ (Fig. 3(c)) overlaps with significant portion of the measured spontaneous emission spectra, ensuring low cavity losses.

2.4. Hybrid integration

To facilitate hybrid integration between the SOA and the wavelength tunable Vernier cavity, both the Si slab waveguide and SSC are used; Si slab waveguide enables mode coupling at the

Optics EXPRESS

III - V/silicon interface whereas the SSC converts the Si slab mode to the strip mode. The Si slab waveguide is angled at 9.8° to ensure compatibility with the III - V waveguide. In order to reduce edge-coupling losses, the facet quality was improved through polishing. Characterization of the laser was carried out by placing the SOA and SiPh chip on 2 different x/y/z precision manual alignment stages, each connected to a thermo-electric controller (TEC); near-field electric field distribution of the III - V waveguide and Si slab waveguide together with its respective sizes are indicated at the inset of Fig. 5(a). The lasing output is collected from the output facet of the SOA via a lensed-fiber [41] (prevent possible reflection into the laser cavity) and connected to the optical spectrum analyzer (OSA, Yokogawa AQ6375) for measuring the lasing spectra or coupled directly into the aperture of the photodetector for laser power characterization taking into account laser divergence angles (on-chip output power). The III - V waveguide-lensed fiber

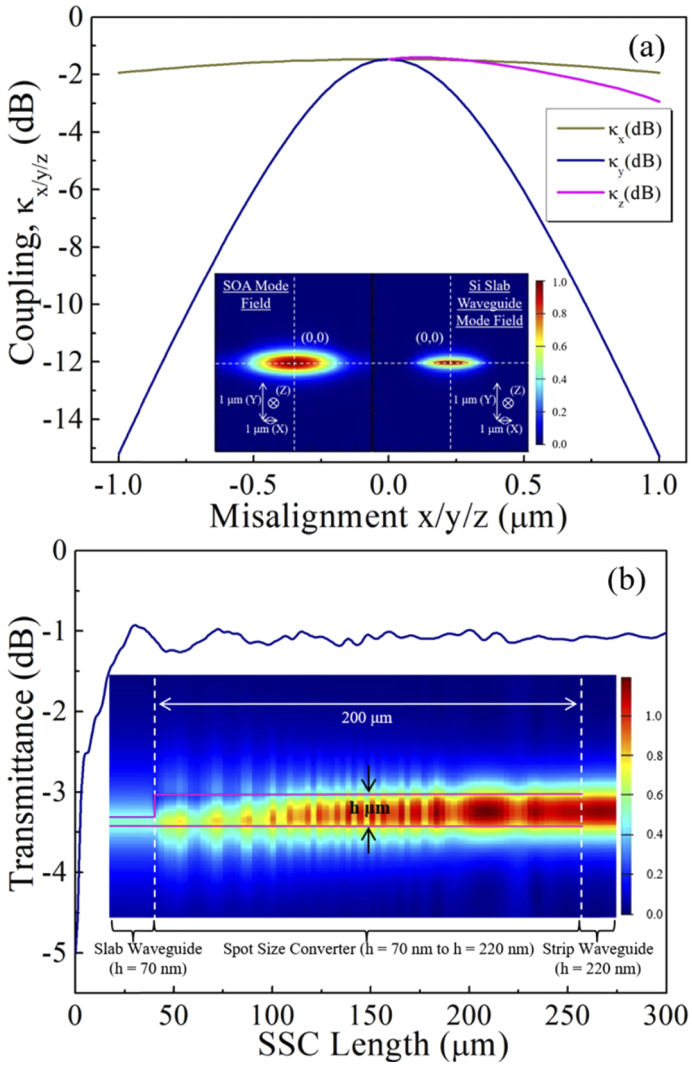

Fig. 5. (a) Simulated SiPh Chip-SOA coupling as a function of misalignment (x/y/z). Inset shows the near-field electric-field distribution of the Si slab and III - V waveguide. (b) Simulated insertion loss of the SSC as a function of coupler length. Inset shows the electric-field distribution (y-z plane) of a 200 μm-long SSC.

Optics EXPRESS

coupling loss is 10 dB; the coupling loss is determined by comparing the difference in the two cases when laser output is coupled directly into the aperture of the photodetector and coupled via a lensed fiber connected to the photodetector. The SOA has a fast and slow-axis divergence angles of 69.3° and 10.8° respectively. Theoretical coupling loss as a function of misalignment between III - V waveguide and Si slab waveguide the in the x/y/z direction is simulated using eigenmode analysis as shown in Fig. 5(a). While a low coupling loss of 1.46 dB can be achieved under optimal alignment condition where the center of both mode fields is aligned together, we find that a 0.5 μm misalignment in the y-direction will result in a high coupling loss of 6 dB. The x and z-direction, on the other hand, are much more resilient; a 0.5 μm misalignment would result in coupling losses of 1.58 and 1.79 dB respectively. As the silicon photonic chip is fabricated in a CMOS process line, the height of the Si slab waveguide and Si taper tip width are fixed at 0.07 and 0.15 μm respectively, leaving the SSC length as the only parameter to optimize. In Fig. 5(b), the length of the SSC [43] is optimized using the 3D-FDTD; when the length of the coupler exceeds 75 μm, low-loss conversion from the slab to strip waveguide can be achieved; the length of the SSC is fabricated to be 200 μm. The inset of Fig. 5(b) shows the electric-field distribution (y-z plane) of the lightwave as it propagates along a 200 μm-long SSC.

3. Experimental performance

The L-I and V-I curves of the laser diode is shown in Figs. 6(a) and 6(b) respectively. The photodetector serves to integrate the sum of the power under the lasing spectra [42].

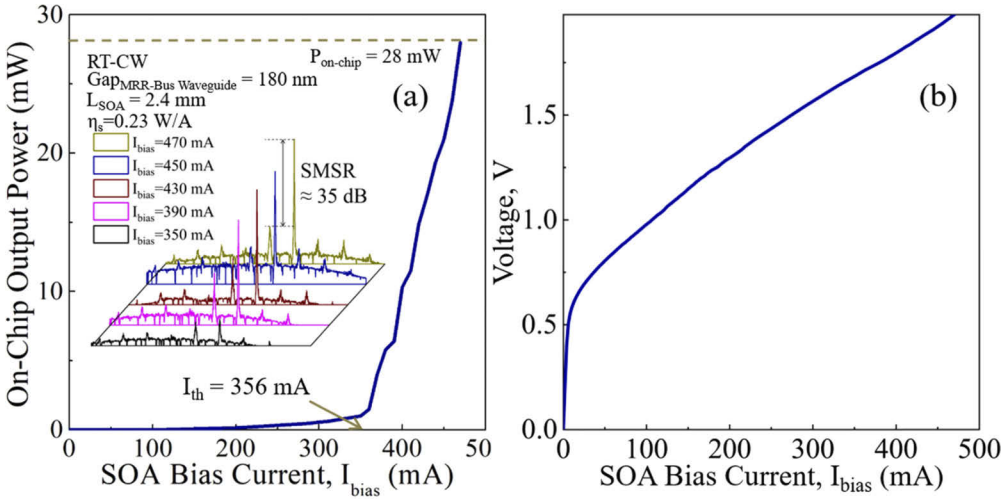

Fig. 6. (a) On-chip output power against I_{bias} (L-I). Inset shows the evolution of the lasing spectra as I_{bias} is increased. (b) Laser I-V.

A threshold current (I_{th}) of 356 mA and slope efficiency (η_s) of 0.232 W/A were obtained under room-temperature continuous-wave (RT-CW) operation, measured by coupling laser output directly into the aperture of a photodetector to determine the on-chip output power. The evolution of the lasing spectra with respect to increasing I_{bias} is shown in the inset; stable single-mode operation with a SMSR of up to 35 dB was obtained at $I_{bias} = 470$ mA. The on-chip output power is 28 mW with a wall plug efficiency (WPE) of 2.3% ($I_{bias} = 450$ mA); electrical power supplied to the TEC is not considered.

Figure 7(a) shows the superimposed lasing spectra ($I_{bias} = 450$ mA) when H_{MRR1} is tuned. By increasing the power supplied to heater 1 (Fig. 7(b)), the wavelength corresponding to the transmittance peak will blue-shift in step-sizes corresponding to FSR_{MRR2} (Fig. 2(a)); lasing will

Optics EXPRESS

occur at the wavelength of lowest loss. The laser achieved a tunable range of 66 nm (1881-1947 nm). While heater 1 is tuned for this demonstration, the opposite is true if heater 2 is tuned; the lasing wavelength will redshift in step-sizes of FSR_{MRR1}.

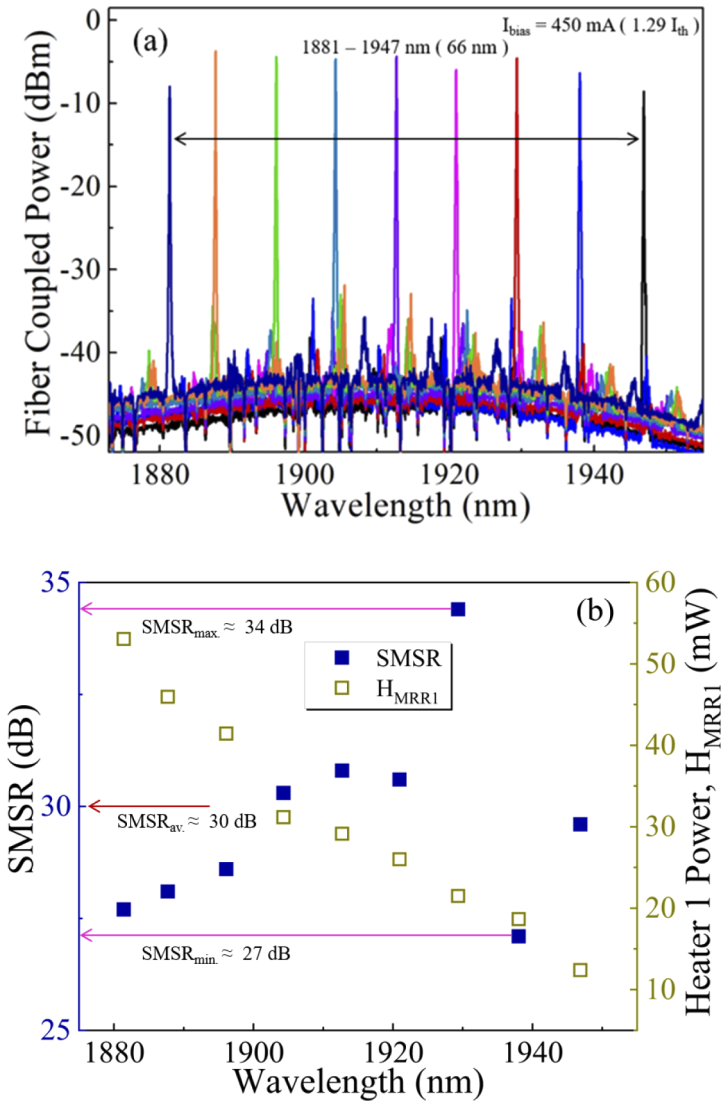

Fig. 7. (a) Superimposed lasing spectra at I_{bias} = 450 mA. (b) SMSR at each lasing wavelength at I_{bias} = 450 mA. H_{MRR1} power required for lasing at corresponding wavelength.

Figure 7(b) shows that the average, maximum and minimum SMSR at each discrete wavelength when I_{bias} = 450 mA is 30, 34 and 27 dB respectively. The variation of SMSR can be attributed to temperature drifts and changes in resistance between the contact probe and pad, subsequently, leading to an imperfect alignment of the 2 MRR resonant peaks.

In view of the channel spacing for commercial WDM systems, by controlling heaters 1 and 2 simultaneously, we demonstrate fine tuning of ~0.8 nm [54], shown in Fig. 8(a). Heater 1 and 2 power values corresponding to the fine tuning are indicated in Fig. 8(b).

Optics EXPRESS

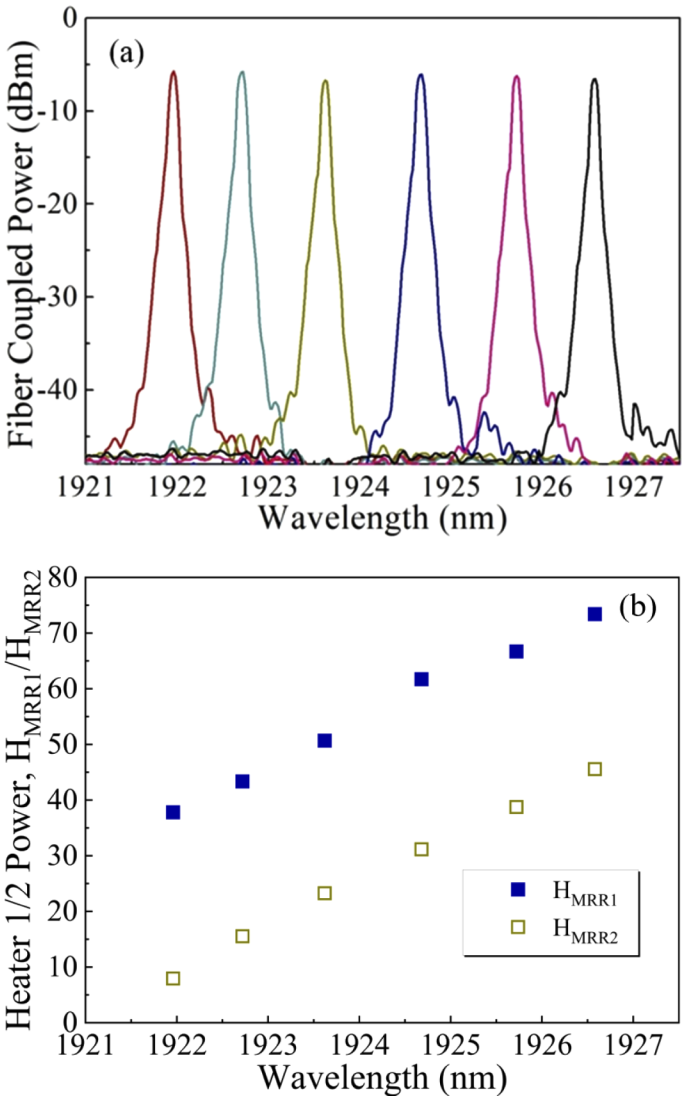

Fig. 8. (a) Superimposed lasing spectra with ~0.8 nm (100 GHz) resolution tuning. (b) H_{MRR1} and H_{MRR2} required for lasing at corresponding wavelength.

4. Conclusion

In summary, we report a SHREC wavelength-tunable laser diode with an operating range of 1881-1947 nm (66 nm), demonstrating good compatibility with the TDFA and HC-PBGF. While having the potential to enable a wide range of technologies such as fiber communications, this wavelength region will find crucial applications in terms of H_2O spectroscopy, optical logic, signal processing as well as enabling the strong optical Kerr effect on Si. Good on-chip output power (28 mW, RT-CW) and tunable range near the 1.9 μm wavelength region was achieved. The laser demonstrated in this work represents a step in the development of silicon photonic devices for the 2 μm waveband. Over the decades, significant strides have been taken at the 1.55 μm waveband. Yet, moving forward, there is still a formidable challenge of how to build on the prior art to push the envelope in view of the rising demand for photonic technologies. This work

Optics EXPRESS

signifies progress to this effect, and further demonstrates the prospects for a 2 μm waveband in a plethora of applications.

Funding

National Research Foundation Singapore (NRFCRP12-2013-04); NTU-A*Star Silicon Technologies Centre of Excellence; NTU-CompoundTek Pte Ltd Research Collaboration Agreement (RCA); National Natural Science Foundation of China (61964007).

Disclosures

The authors declare that there are no conflicts of interest related to this article.

References

1. K. Nagayama, M. Kakui, M. Matsui, T. Saitoh, and Y. Chigusa, "Ultra-low-loss (0.1484 dB/km) pure silica core fibre and extension of transmission distance," Electron. Lett. **38**(20), 1168–1169 (2002).
2. E. Desurvire, *Erbium-doped fiber amplifiers: principles and applications* (Wiley-Interscience: New York, NY, 2002).
3. C. Brackett, "Dense wavelength division multiplexing networks: principles and applications," IEEE J. Select. Areas Commun. **8**(6), 948–964 (1990).
4. S. J. Savory, "Digital Coherent Optical Receivers: Algorithms and Subsystems," IEEE J. Sel. Top. Quantum Electron. **16**(5), 1164–1179 (2010).
5. D. J. Richardson, "Filling the Light Pipe," Science **330**(6002), 327–328 (2010).
6. L.-W. Luo, N. Ophir, C. P. Chen, L. H. Gabrielli, C. B. Poitras, K. Bergmen, and M. Lipson, "WDM-compatible mode-division multiplexing on a silicon chip," Nat. Commun. **5**(1), 3069 (2014).
7. B. Inan, B. Spinnler, F. Ferreira, D. V. D. Borne, A. Lobato, S. Adhikari, V. A. J. M. Sleiffer, M. Kuschnerov, N. Hanik, and S. L. Jansen, "DSP complexity of mode-division multiplexed receivers," Opt. Express **20**(10), 10859–10869 (2012).
8. A. Lobato, J. Rabe, F. Ferreira, M. Kuschnerov, B. Spinnler, and B. Lankl, "Near-ML detection for MDL-impaired few-mode fiber transmission," Opt. Express **23**(8), 9589–9601 (2015).
9. F. Poletti, N. V. Wheeler, M. N. Petrovich, N. Baddela, E. N. Fokoua, J. R. Hayes, D. R. Gray, Z. Li, R. Slavík, and D. J. Richardson, "Towards high-capacity fibre-optic communications at the speed of light in vacuum," Nat. Photonics **7**(4), 279–284 (2013).
10. M. N. Petrovich, F. Poletti, J. P. Wooler, A. Heidt, N. Baddela, Z. Li, D. Gray, R. Slavík, F. Parmigiani, N. Wheeler, J. Hayes, E. Numkam, L. Grűner-Nielsen, B. Pálsdóttir, R. Phelan, B. Kelly, J. O'Carroll, M. Becker, N. Macsuibhne, J. Zhao, F. G. Gunning, A. Ellis, P. Petropoulos, S. Alam, and D. Richardson, "Demonstration of amplified data transmission at 2 μm in a low-loss wide bandwidth hollow core photonic bandgap fiber," Opt. Express **21**(23), 28559–28569 (2013).
11. P. J. Roberts, F. Couny, H. Sabert, B. J. Mangan, D. P. Williams, L. Farr, M. W. Mason, A. Tomlinson, T. A. Birks, J. C. Knight, and P. S. J. Russell, "Ultimate low loss of hollow-core photonic crystal fibres," Opt. Express **13**(1), 236–244 (2005).
12. B. J. Mangan, L. Farr, A. Langford, P. J. Roberts, D. P. Williams, F. Couny, M. Lawman, M. Mason, S. Coupland, R. Flea, H. Sabert, T. A. Birks, J. C. Knight, and P. St. J. Russel, "Low loss (1.7 dB/km) hollow core photonic bandgap fiber," in *Optical Fiber Communication Conference*, (Optical Society of America, 2004).
13. Z. Li, A. M. Heidt, J. M. O. Daniel, Y. Jung, S. U. Alam, and D. J. Richardson, "Thulium-doped fiber amplifier for optical communications at 2 μm," Opt. Express **21**(8), 9289–9297 (2013).
14. Z. Li, A. M. Heidt, N. Simakov, Y. Jung, J. M. O. Daniel, S. U. Alam, and D. J. Richardson, "Diode-pumped wideband thulium-doped fiber amplifiers for optical communications in the 1800–2050nm window," Opt. Express **21**(22), 26450–26455 (2013).
15. H. Zhang, N. Kavanagh, Z. Li, J. Zhao, N. Ye, Y. Chen, N. V. Wheeler, J. P. Wooler, J. R. Hayes, S. R. Sandoghchi, F. Poletti, M. N. Petrovich, S. U. Alam, R. Phelan, J. O'Carroll, B. Kelly, L. Grüner-Nielsen, D. J. Richardson, B. Corbett, and F. C. G. Gunning, "100 Gbit/s WDM transmission at 2 μm: transmission studies in both low-loss hollow core photonic bandgap fiber and solid core fiber," Opt. Express **23**(4), 4946–4951 (2015).
16. H. Zhang, M. Gleeson, N. Ye, N. Pavarelli, X. Ouyang, J. Zhao, N. Kavanagh, C. Robert, H. Yang, P. E. Morrissey, K. Thomas, A. Gocalinska, Y. Chen, T. Bradley, J. P. Wooler, J. R. Hayes, E. N. Fokoua, Z. Li, S. U. Alam, F. Poletti, M. N. Petrovich, D. J. Richardson, B. Kelly, J. O'Carroll, R. Phelan, E. Pelucchi, P. O'Brien, F. Peters, B. Corbett, and F. Gunning, "Dense WDM transmission at 2 μm enabled by an arrayed waveguide grating," Opt. Lett. **40**(14), 3308–3311 (2015).
17. T. Milde, C. Assmann, A. Jimenez, M. Honsberg, J. O'Gorman, W. Schade, and J. Sacher, "Single mode GaSb diode lasers for sensor applications in a long wavelength regime," Appl. Opt. **56**(31), H45–H50 (2017).
18. K. Scholle, S. Lamrini, P. Koopmann, and P. Fuhrberg, *Frontiers in Guided Wave Optics and Optoelectronics: 2 μm Sources and Their Possible Applications* (Intech Open, 2010).

Optics EXPRESS

19. T. M. Taczak and D. K. Killinger, "Development of a tunable, narrow-linewidth, cw 2066-μm Ho:YLF laser for remote sensing of atmospheric CO_2 and H_2O," Appl. Opt. **37**(36), 8460–8476 (1998).
20. P. Dong, S. Liao, D. Feng, H. Liang, D. Zheng, R. Shafiiha, C.-C. Kung, W. Qian, G. Li, X. Zheng, A. V. Krishnamoorthy, and M. Asghari, "Low V_{pp}, ultralow-energy, compact, high-speed silicon electro-optic modulator," Opt. Express **17**(25), 22484–22490 (2009).
21. E. Timurdogan, C. M. Sorace-Agaskar, J. Sun, E. S. Hosseini, A. Biberman, and M. R. Watts, "An ultralow power athermal silicon modulator," Nat. Commun. **5**(1), 4008 (2014).
22. D. Dai, Z. Wang, and J. E. Bowers, "Ultrashort broadband polarization beam splitter based on an asymmetrical directional coupler," Opt. Lett. **36**(13), 2590–2592 (2011).
23. W. Bogaerts, P. De Heyn, T. V. Vaerenbergh, K. De Vos, S. K. Selvaraja, T. Claes, P. Dumon, P. Bienstman, D. Van Thourhout, and R. Baets, "Silicon microring resonators," Laser Photonics Rev. **6**(1), 47–73 (2012).
24. D. Celo, D. J. Goodwill, J. Jiang, P. Dumais, C. Zhang, F. Zhao, X. Tu, C. Zhang, S. Yan, J. He, M. Li, W. Liu, Y. Wei, D. Geng, H. Mehrvar, and E. Bernier, "32 × 32 Silicon Photonic Switch," in *21st OptoElectronics and Communications Conference, International Conference on Photonics in Switching*, (2016).
25. D. Benedikovic, L. Virot, G. Aubin, F. Amar, B. Szelag, B. Karakus, J.-M. Hartmann, C. Alonso-Ramos, X. L. Roux, P. Crozat, E. Cassan, D. Marris-Morini, C. Baudot, F. Boeuf, J.-M. Fédéli, C. Kopp, and L. Vivien, "25 Gbps low-voltage hetero-structured silicon-germanium waveguide pin photodetectors for monolithic on-chip nanophotonic architectures," Photonics Res. **7**(4), 437–444 (2019).
26. P. De Heyn, D. Vermeulen, T. Van Vaerenbergh, G. Kuyken, and D. Van Thourhout, "Ultra-high Q and finesse all-pass microring resonators on Silicon-on-Insulator using rib waveguides," in *16th European Conference on Integrated Optics*, (2012).
27. J. Sun, R. Kumar, M. Sakib, J. B. Driscoll, H. Jayatilleka, and H. Rong, "A 128 Gb/s PAM4 Silicon Microring Modulator With Integrated Thermo-Optic Resonance Tuning," J. Lightwave Technol. **37**(1), 110–115 (2019).
28. J. X. B. Sia, W. Wang, X. Guo, J. Zhou, Z. Zhang, M. S. Rouifed, X. Li, Z. L. Qiao, C. Y. Liu, C. Littlejohns, G. T. Reed, and H. Wang, "Mid-Infrared, Ultra-Broadband, Low-Loss, Compact Arbitrary Power Splitter Based on Adiabatic Mode Evolution," IEEE Photonics J. **11**(2), 1–11 (2019).
29. F. Gunning and B. Corbett, "Time to Open the 2-μm Window?" Opt. Photonics News **30**(3), 42 (2019).
30. W. Cao, D. Hagan, D. J. Thomson, M. Nedeljkovic, C. G. Littlejohns, A. Knights, S. Alam, J. Wang, F. Gardes, W. Zhang, S. Liu, K. Li, M. S. Rouifed, G. Xin, W. Wang, H. Wang, G. T. Reed, and G. Z. Mashanovich, "High-speed silicon modulators for the 2 μm band," Optica **5**(9), 1055–1062 (2018).
31. J. J. Ackert, D. J. Thomson, L. Shen, A. C. Peacock, P. E. Jessop, G. T. Reed, G. Z. Mashanovich, and A. P. Knights, "High-speed detection at two micrometres with monolithic silicon photodiodes," Nat. Photonics **9**(6), 393–396 (2015).
32. D. Liu, H. Wu, and D. Dai, "Silicon multimode waveguide grating filter at 2 μm," J. Lightwave Technol. **37**(10), 2217–2222 (2019).
33. J. Li, Y. Liu, Y. Meng, K. Xu, J. Du, F. Wang, Z. He, and Q. Song, "2-μm Wavelength Grating Coupler, Bent Waveguide, and Tunable Microring on Silicon Photonic MPW," IEEE Photonics Technol. Lett. **30**(5), 471–474 (2018).
34. Z. Ruan, L. Shen, S. Zheng, A. Wang, Y. Long, N. Zhou, and J. Wang, "Subwavelength grating slot (SWGS) waveguide at 2 μm for chip-scale data transmission," Nanophotonics **7**(5), 865–871 (2018).
35. D. E. Hagan and A. P. Knights, "Mechanisms for optical loss in SOI waveguides for mid-infrared wavelengths around 2μm," J. Opt. **19**(2), 025801 (2017).
36. T. Komljenovic, M. Davenport, J. Hume, A. Y. Liu, C. T. Santis, A. Spott, S. Srinivasan, E. J. Stanton, C. Zhang, and J. E. Bowers, "Heterogenous Silicon Photonic Integrated Circuits," J. Lightwave Technol. **34**(1), 20–35 (2016).
37. T. Feng, T. Hosoda, L. Shterengas, A. Stein, G. Kipshidze, and G. Belenky, "Two-Step Narrow Ridge Cascade Diode Lasers Emitting Near 2 μm," IEEE Photonics Technol. Lett. **29**(6), 485–488 (2017).
38. K. Vizbaras, E. Dvinelis, I. Šimonytė, A. Trinkūnas, M. Greibus, R. Songaila, T. Žukauskas, M. Kaušylas, and A. Vizbaras, "High power continuous-wave GaSb-based superluminescent diodes as gain chips for widely tunable laser spectroscopy in the 1.95–2.45 μm wavelength range," Appl. Phys. Lett. **107**(1), 011103 (2015).
39. D. Huang, M. A. Tran, J. Guo, J. Peters, T. Komljenovic, A. Malik, P. A. Morton, and J. E. Bowers, "High-power sub-kHz linewidth lasers fully integrated on silicon," Optica **6**(6), 745–752 (2019).
40. R. Wang, B. Haq, S. Sprengel, A. Malik, A. Vasiliev, G. Boehm, I. Simonyte, K. Vizbaras, J. Van Campenhout, R. Baets, M. Amann, and G. Roelkens, "Widely Tunable III-V/Silicon Lasers for Spectroscopy in the Short-Wave Infrared," IEEE J. Sel. Top. Quantum Electron. **25**(6), 1–12 (2019).
41. T. Kita, R. Tang, and H. Yamada, "Narrow Spectral Linewidth Silicon Photonic Wavelength Tunable Laser Diode for Digital Coherent Communication System," IEEE J. Sel. Top. Quantum Electron. **22**(6), 23–34 (2016).
42. T. Kita, R. Tang, and H. Yamada, "Compact silicon photonic wavelength-tunable laser diode with ultra-wide wavelength tuning range," Appl. Phys. Lett. **106**(11), 111104 (2015).
43. S. Yang, Y. Zhang, D. W. Grund, G. A. Ejzak, Y. Liu, A. Novack, D. Prather, A. E.-J. Lim, G.-Q. Lo, T. Baehr-Jones, and M. Hochberg, "A single adiabatic microring-based laser in 220 nm silicon-on-insulator," Opt. Express **22**(1), 1172–1180 (2014).
44. N. Fujioka, T. Chu, and M. Ishizaka, "Compact and Low Power Consumption Hybrid Integrated Wavelength Tunable Laser Module Using Silicon Waveguide Resonators," J. Lightwave Technol. **28**(21), 3115–3120 (2010).

Optics EXPRESS

45. H. Guan, A. Novack, T. Galfsky, Y. Ma, S. Fathololoumi, A. Horth, T. N. Huynh, J. Roman, R. Shi, M. Caverley, Y. Liu, T. Baehr-Jones, K. Bergman, and M. Hochberg, "Widely-tunable, narrow-linewidth III-V/silicon hybrid external-cavity laser for coherent communication," Opt. Express **26**(7), 7920–7933 (2018).
46. T. Chu, N. Fujioka, and M. Ishizaka, "Compact, lower-power-consumption wavelength tunable laser fabricated with silicon photonic-wire waveguide micro-ring resonators," Opt. Express **17**(16), 14063–14068 (2009).
47. R. Wang, A. Malik, I. Šimonytė, A. Vizbaras, K. Vizbaras, and G. Roelkens, "Compact GaSb/silicon-on-insulator 2.0x μm widely tunable external cavity lasers," Opt. Express **24**(25), 28977–28986 (2016).
48. J. X. B. Sia, W. Wang, Z. Qiao, X. Li, X. Guo, J. Zhou, Z. Zhang, C. Littlejohns, C. Liu, G. T. Reed, and H. Wang, "Compact, ultra-tunable InGaSb/AlGaAsSb Si external cavity laser at the Mid-Infrared (MIR)," in *Conference on Lasers and Electro-Optics*, (Optical Society of America, 2019).
49. A. D. Bristow, N. Rotenberg, and H. M. V. Driel, "Two-photon absorption and Kerr coefficients of silicon for 850–2200 nm," Appl. Phys. Lett. **90**(19), 191104 (2007).
50. M. Melieres and C. Marechal, *Climate Change: Past, Present and Future* (Wiley Blackwell, 2015), Chap. 7.
51. X. Li, H. Wang, Z. Qiao, X. Guo, G. I. Ng, Y. Zhang, Z. Niu, C. Tong, and C. Liu, "Modal gain characteristics of a 2 μm InGaSb/AlGaAsSb passively mode-locked quantum well laser," Appl. Phys. Lett. **111**(25), 251105 (2017).
52. C. Liu, H. Wang, Q. Meng, B. Gao, and K. S. Ang, "Modal Gain and Photoluminescence Investigation of Two-State Lasing in GaAs-Based 1.3 μm InAs/InGaAs Quantum Dot Lasers," Appl. Phys. Express **6**(10), 102702 (2013).
53. X. Li, H. Wang, Z. Qiao, Y. Liao, Y. Zhang, Y. Xu, Z. Niu, C. Tong, and C. Liu, "Temperature- and current-dependent spontaneous emission study on 2 μm InGaSb/AlGaAsSb quantum well lasers," Jpn. J. Appl. Phys. **56**(5), 050310 (2017).
54. Everlz, "9000WDM Dense WDM 1RU Optical Unit," https://evertz.com/products/9000DWDM